

LETTER • OPEN ACCESS

Have human activities changed the frequencies of absolute extreme temperatures in eastern China?

To cite this article: Jun Wang *et al* 2018 *Environ. Res. Lett.* **13** 014012

View the [article online](#) for updates and enhancements.

You may also like

- [Heterogeneous spring phenology shifts affected by climate: supportive evidence from two remotely sensed vegetation indices](#)
Xiyun Xu, William J Riley, Charles D Koven *et al.*
- [New satellite climate data records indicate strong coupling between recent frozen season changes and snow cover over high northern latitudes](#)
Youngwook Kim, J S Kimball, D A Robinson *et al.*
- [Enhanced nighttime heatwaves over African urban clusters](#)
Eghosa Igun, Xiyun Xu, Zitong Shi *et al.*



The Breath Biopsy® Guide
Fourth edition

DOWNLOAD THE FREE E-BOOK

BREATH BIOPSY

OWLSSTONE MEDICAL

Environmental Research Letters



LETTER

Have human activities changed the frequencies of absolute extreme temperatures in eastern China?

OPEN ACCESS

RECEIVED

2 September 2017

REVISED

13 October 2017

ACCEPTED FOR PUBLICATION

17 October 2017

PUBLISHED

10 January 2018

Jun Wang^{1,4} , Simon F B Tett², Zhongwei Yan^{1,3} and Jinming Feng¹¹ Key Laboratory of Regional Climate-Environment for Temperate East Asia, Institute of Atmospheric Physics, Chinese Academy of Sciences, Beijing, People's Republic of China² National Center for Atmospheric Sciences, Climate & School of Geosciences, The University of Edinburgh, Edinburgh, United Kingdom³ University of Chinese Academy of Sciences, Beijing, People's Republic of China⁴ Author to whom any correspondence should be addressed.E-mail: wangjun@tea.ac.cn**Keywords:** extreme temperatures, human activities, greenhouse gases, detection and attributionSupplementary material for this article is available [online](#)

Original content from this work may be used under the terms of the [Creative Commons Attribution 3.0 licence](#).

Any further distribution of this work must maintain attribution to the author(s) and the title of the work, journal citation and DOI.

**Abstract**

Extreme temperatures affect populous regions, like eastern China, causing substantial socio-economic losses. It is beneficial to explore whether the frequencies of absolute or threshold-based extreme temperatures have been changed by human activities, such as anthropogenic emissions of greenhouse gases (GHGs). In this study, we compared observed and multi-model-simulated changes in the frequencies of summer days, tropical nights, icy days and frosty nights in eastern China for the years 1960–2012 by using an optimal fingerprinting method. The observed long-term trends in the regional mean frequencies of these four indices were $+2.36$, $+1.62$, -0.94 , -3.02 days decade⁻¹. The models performed better in simulating the observed frequency change in daytime extreme temperatures than nighttime ones. Anthropogenic influences are detectable in the observed frequency changes of these four temperature extreme indices. The influence of natural forcings could not be detected robustly in any indices. Further analysis found that the effects of GHGs changed the frequencies of summer days (tropical nights, icy days, frosty nights) by $+3.48 \pm 1.45$ ($+2.99 \pm 1.35$, -2.52 ± 1.28 , -4.11 ± 1.48) days decade⁻¹. Other anthropogenic forcing agents (dominated by anthropogenic aerosols) offset the GHG effect and changed the frequencies of these four indices by -1.53 ± 0.78 , -1.49 ± 0.94 , $+1.84 \pm 1.07$, $+1.45 \pm 1.26$ days decade⁻¹, respectively. Little influence of natural forcings was found in the observed frequency changes of these four temperature extreme indices.

1. Introduction

Extreme temperatures cause substantial risk to human health, agriculture and the ecosystem (Field *et al* 2012). The associations between human activities and extreme temperatures are often studied, especially after so many places on the globe have encountered unprecedented extreme weather, such as Europe in the summer of 2003 (Stott *et al* 2004) and eastern USA in the winter of 2014 (Trenary *et al* 2015). Extreme temperatures spread over central-eastern China in the summer of 2013 and eastern China in the winter of 2016 caused unprecedented death tolls and socio-economical losses (Sun *et al* 2014, Wang *et al* 2017, Qian *et al* 2017). Exploring the roles of external drivers in the frequency changes of extreme temperatures is urgent, in order

to provide reliable projections of extreme temperatures and indicative references for the adaptation and mitigation of regional climate change.

Previous detection and attribution studies focused on the changes in annual maxima/minima of daily temperatures (Christidis *et al* 2011, 2015, Wen *et al* 2013, Kim *et al* 2016, Yin *et al* 2017) and percentile-based extreme temperatures (Christidis *et al* 2005, Morak *et al* 2011, 2013, Lu *et al* 2016), and indicated that the influence of human activities has contributed to these changes at global and regional scales (Stott *et al* 2016). A pioneering study conducted by Hegerl *et al* (2004) examined whether the changes in extreme temperatures are detectable in a perfect model configuration. They found that the difficulty in detecting changes in extreme temperatures is no more than the

detection of changes in its mean state. Christidis *et al* (2005) first used the optimal fingerprinting method to detect the anthropogenic influences on the changes in extreme temperatures during the second half of the last century. As for China, Wen *et al* (2013) and Yin *et al* (2017) used an optimal detection method to detect human influence on the changes in annual maxima and minima of daily temperatures in China. They found that anthropogenic influences are detectable in the changes of extreme temperatures in China. Lu *et al* (2016) conducted detection analysis on the frequencies of percentile-based extreme temperatures in China during the period 1958–2002, and also found clear anthropogenic signals in the observed frequency changes in relatively warmer and colder days and nights.

However, socio-economic stress from extreme temperatures is mostly felt through the changes in absolute or threshold-based extreme high or low temperatures. We focus especially on absolute extreme temperatures, precisely because of their practical significance. Threshold-based extreme temperatures directly contribute to increased discomfort and mortality rates, and agricultural and hydrological disaster losses (Basu and Samet 2002, Bai *et al* 2014, Lesk *et al* 2016). Current detection and attribution studies require signals from climate model simulations. One of the major challenges faced by the attribution studies of changes in threshold-based extreme temperatures is that current climate models cannot well represent the mean state of surface air temperature at regional scales (Sun *et al* 2015). Simulated frequency changes in the threshold-based extreme temperatures tend to be sensitive to this model potential bias. Therefore, before calculating the frequency of these extreme temperatures, we need to evaluate the model performance. In addition, changes in daily maximum (T_{\max}) and minimum (T_{\min}) temperatures are dominated by the variations of surface solar radiation and net longwave radiation, respectively (Zhou and Wang 2016). Human influence on the changes in the daytime and nighttime temperatures is unlikely to be identical, as is the case for extreme temperatures.

In this study, we choose four indices of absolute extreme temperatures as defined by the Expert Team on Climate Change Detection and Indices (ETCCDI; www.climdex.org/indices.html) and previous studies (Alexander *et al* 2006, Zhang *et al* 2011) and study the frequency changes in daytime and nighttime extreme temperatures separately. We measure the days with T_{\max} higher than 25 °C as summer days and the night with T_{\min} higher than 20 °C as tropical nights. We also count the days with T_{\max} and T_{\min} lower than 0 °C as icy days and frosty nights, respectively. We employ an optimal fingerprinting technique to detect and attribute the influences of human activities, including greenhouse gases and other anthropogenic forcings (dominated by anthropogenic aerosols), and natural external forcings (combined effect of total solar irradiance variations and

aerosols from volcanic eruptions), on these long-term changes.

2. Data and methods

2.1. Observations

We use a newly homogenized daily T_{\max} and T_{\min} dataset observed at 753 Chinese meteorological stations for 1960–2012 (figure S1, available at stacks.iop.org/ERL/13/014012/mmedia). The temperature observations we use have been quality-controlled and adjusted for most non-climatic biases due to the changes in the local observing system, such as station relocation (Li and Yan 2009, Li *et al* 2016).

Since the horizontal resolutions of climate models are in the range of 1°–3°, we divide the mainland of eastern China into 2° × 2° resolution grid boxes and construct a regional gridded temperature dataset using available observations within each grid box. Specifically, we first calculate the climatological mean annual cycle (base period: 1960–2012) and daily temperature anomalies at each station. Given that temperature is dependent on elevation, for the boxes where topography has a wide range and stations are unevenly distributed, there might be certain deviation in the extreme temperatures if the gridded temperature is developed by simple averaging of the individual station within each grid box. Hence, we need to correct the elevation-related bias in the temperature mean state within each grid box. Considering the lapse rate of near-surface air temperature is time-varying and region-dependent, use of a fixed temperature lapse rate could be problematic on the complex terrains in China. Following Li *et al* (2013), we divide the whole mainland China into 24 sub-regions (figure S1). We use the multiple linear regression method including the effects of latitude, longitude and elevation to estimate the lapse rates of T_{\max} and T_{\min} for each sub-region and each month (figure S2). The terrain-based global 0.25° × 0.25° land elevation and ocean depth dataset (TBASE) (http://research.jisao.washington.edu/data_sets/elevation/) is applied to estimate the averaged elevation within each grid box (figure S3). The local elevation bias in climatological mean annual cycle of the individual station is adjusted based on the spatiotemporal-varying temperature lapse rates. The final gridded dataset is obtained by adding the station average temperature anomalies to the station average elevation-bias-corrected climatological mean annual cycle for each grid box. Furthermore, to estimate the regional averages precisely, we establish a set of areal weights of land fraction by considering their latitude-dependent feature and the influence of coasts and islands (figure S4).

2.2. Model simulations

We use the CMIP5 simulations to estimate the responses of extreme temperatures to external forcings

Table 1. The CMIP5 models used in the optimal fingerprinting analyses. Numbers represent the ensemble sizes of the ALL, NAT and GHG simulations, the years of CTL simulations, and the spatial resolutions of atmospheric component of climate models. Aerosol species considered in each model are also shown.

Model	ALL	NAT	GHG	CTL	Spatial resolution (lat and lon)		Aerosol species
CanESM2	5	5	5	636	2.7906°	2.8125°	SO ₄ , BC, OA, DS, SS
CNRM-CM5	10	6	6	636	1.4008°	1.4063°	SO ₄ , BC, OA, DS, SS
CSIRO-Mk3-6-0	10	5	5	424	1.8653°	1.875°	SO ₄ , BC, OA, DS, SS
HadGEM2-ES	4	4	4	530	1.25°	1.875°	SO ₄ , AN, BC, OA, DS, SS
IPSL-CM5A-LR	4	3	3	954	1.8947°	3.75°	SO ₄ , BC, OA, DS, SS
Total	33	23	23	3180			

Notes: SO₄, sulfate; AN, ammonium nitrate; BC, black carbon; OA, organic carbon (including primary and secondary organic carbon); DS, dust; SS, sea salt.

and the internal climate variability. Table 1 lists all the available CMIP5 models used in this study. All the experiments with specific forcings have three or more members and produce daily outputs. We first evaluate the skill of climate models with ALL forcing in simulating the climatological mean of T_{\max} and T_{\min} . As shown in figures S5 and S6, climate models tend to perform better over eastern China than western China. There are two explanations for this discrepancy: (1) the station density in western China is much lower than eastern China (figure S1); (2) the topography in western China is much more complex than eastern China, which is poorly captured in models with resolutions of around 1–3 degrees (figure S3). The gridded temperature values can be affected seriously by individual station with local effects. We focus our analysis on eastern China (east of 105 °E) also because the majority of China's people live in the eastern part of the country.

We calculate the time series of simulated regional mean frequency of extreme temperatures in eastern China, and compare them with the observed ones (figure S7). Results illustrate a good consistency between the observed and simulated frequencies of summer days and tropical nights in eastern China, though models tend to overestimate the frequencies of icy days and frosty nights in eastern China by on average 33.6% (14.1 days) and 13.8% (14.4 days), respectively. However, in western China, the spread of simulated frequencies of extreme temperatures is very large (figure S8). It implies that CMIP5 models can hardly capture the mean state and variability of surface air temperature in western China. Based on these evaluations, we focus on eastern China in this study.

We use 32 simulations from five models driven by combined anthropogenic and natural forcing (ALL); 23 simulations from five models driven by natural forcing only (NAT) and greenhouse gas forcing only (GHG) (table 1). All simulations end in 2012. More recent years are not included in this study, as most of the model simulations required for the detection analyses ended in 2012. It is assumed that the temperature extreme responses to historical anthropogenic (ANT) and NAT forcings are linearly additive and the difference between the ALL and NAT responses can be estimated as an ANT response. Annual anomalies, with respect to 1960–2012, are computed from

the resulting regional average frequency of extreme temperatures from observations and individual model runs, using the same sets of space data masks and areal weights. We compute the ensemble means for individual models and then average the ensemble means to give the expected multi-model response to large-scale external forcings. Thus, the patterns we consider are the annual anomalies of the frequency of extreme temperatures.

2.3. Optimal fingerprinting method

We use an optimal fingerprinting method in which observations (y) are expressed as a sum of scaled model-simulated fingerprint patterns (X) plus internal climate variability (ϵ) as $y = X\beta + \epsilon$. The scaling factors β adjust the magnitude of the fingerprints to best match the observations. The multi-model ensemble averages of forced (ALL, GHG and NAT) simulations are used to estimate the fingerprints, and the pre-industrial control (CTL) simulations are used to estimate internal climate variability. The regression is fitted based on equation (4) in Allen and Tett (1999): $\tilde{\beta} = (X^T C_N^{-1} X)^{-1} X^T C_N^{-1} Y$. We compute non-overlapping 3-year-mean time series of the multi-model-simulated regional mean frequency of extreme temperatures as the forced response or signal for the specific forcing (X), which includes 18 data values for the period 1960–2012. Observations are processed in the same way as the simulations. Fitting and testing the regression models need two independent estimates of the inversed covariance structure of internal climate variability (C_N^{-1}). We use the CTL simulations and the inter-ensemble difference from forced simulations to estimate them. Time series from CTL simulations are divided into 60 non-overlapping 53 year chunks and similarly masked to be in accord with observations in space. Additional 79 non-overlapping 53 year chunks are constructed using inter-ensemble differences from forced simulations (ALL: 33; GHG: 23; NAT: 23). We separate each set of chunks from CTL simulations or forced simulations into two groups sequentially. The first group of chunks is used to pre-whiten the data and the second group is used for the uncertainty analysis on the estimation of scaling factors ($\tilde{\beta}$). Instead of decreasing the dimension via a projection on the first k leading empirical orthogonal functions, we use a regularized

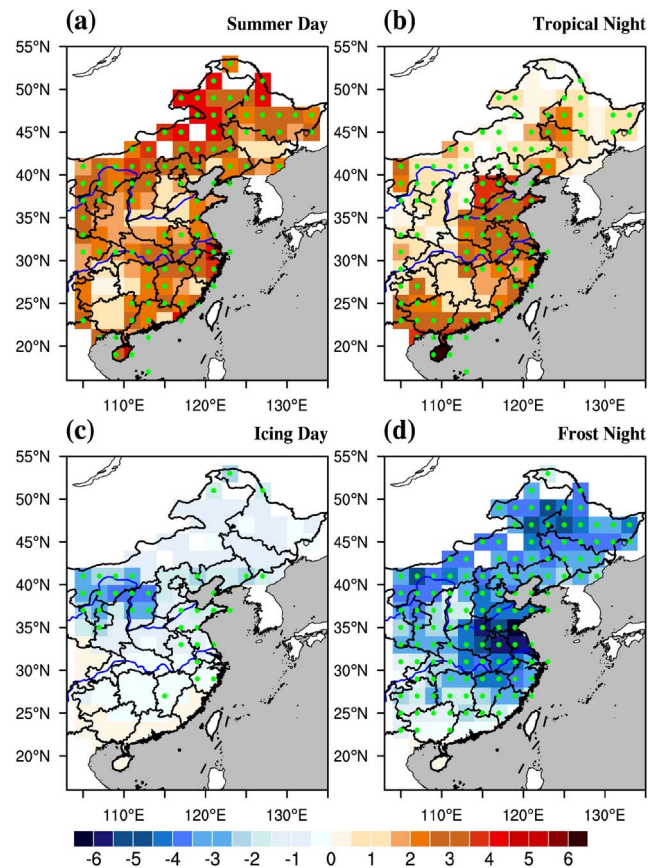


Figure 1. Observed trends (days decade⁻¹) in the frequencies of (a) summer days, (b) tropical nights, (c) icy days, and (d) frosty nights in eastern China during the years of 1960–2012. Green dots represent the grid boxes where the trend is significant at the 95% confidence level. Linear trends in the frequencies of extreme temperatures were estimated by using the ordinary least squares method, with Student's *t* test for testing statistical significance.

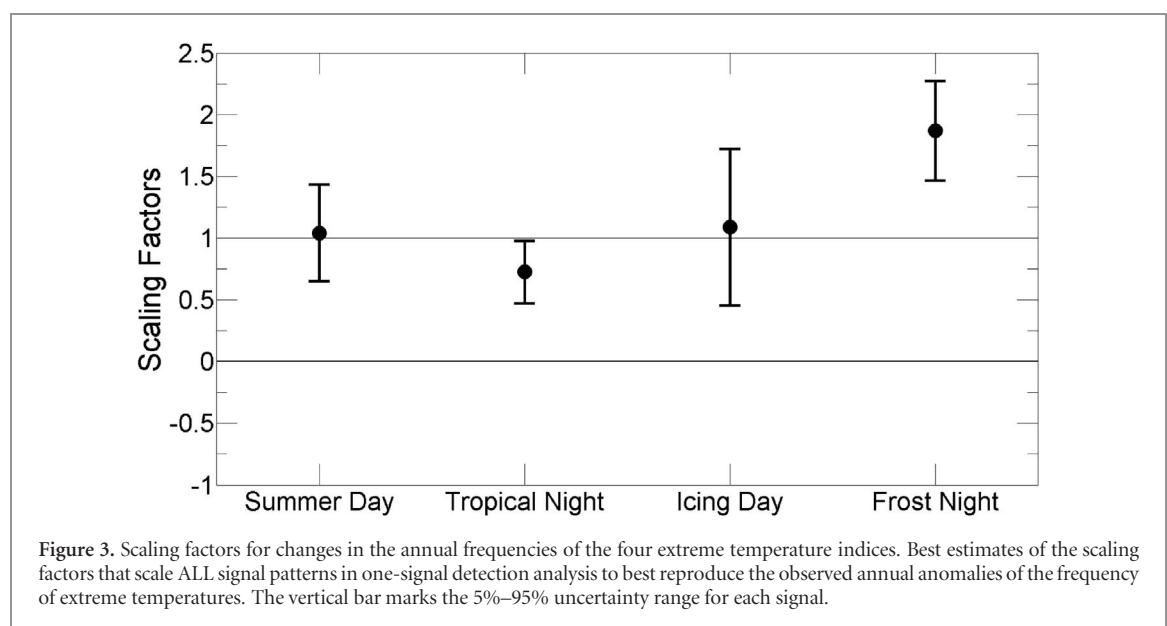
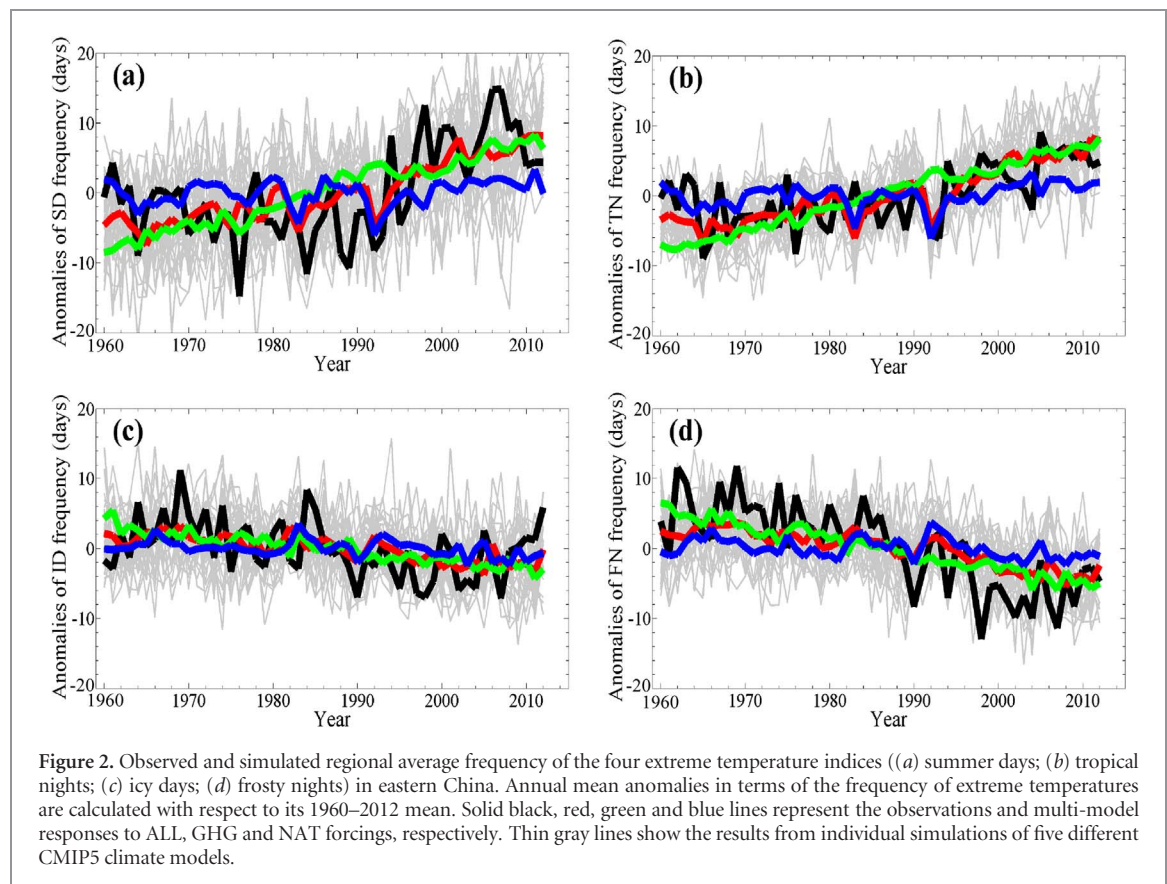
estimate of the covariance matrix of the internal climate variability (Ribes *et al* 2009). Regularized estimation of the covariance matrix can avoid the underestimation of the lowest eigenvalues that occurs in original covariance matrix and ensure the covariance matrix is full rank (Ribes *et al* 2013). We apply equation (19) provided by Allen and Tett (1999) to conduct residual consistency checks to detect model inadequacy. The results show that all the regression models can pass this test, which means that climate models are able to simulate the internal variability of the frequency of extreme temperatures in eastern China reasonably well.

Based on equations (6) and (7) in Allen and Tett (1999), we estimate the variance-covariance matrices of the internal variability noise by using the first set of non-overlapping 53 year chunks. We obtain the 5%–95% uncertainty range of scaling factors by assuming that the internal variability noise is normally distributed. To estimate the probability distribution functions of the contributions from different forcing agents, we generate random samples of 10 000 000 values from the normal distribution of estimated scaling factors and multiply the forced trends in different signals by these random numbers.

3. Results

3.1. Patterns and one-signal detection analysis

Figure 1 shows the spatial distributions of observed trends in the frequencies of the four extreme temperature indices. Summer days have increased significantly over the northeastern China (120–135°E, 40–55°N; +2.67 days decade⁻¹) and the middle and lower reaches of the Yangtze River (110–125°E, 28–32°N; +2.99 days decade⁻¹). The occurrences of tropical nights increased mainly over the Yangtze–Huaihe River basin (115–125°E, 28–34°N; +2.62 days decade⁻¹) and part of southern China (105–115°E, 18–24°N; +3.91 days decade⁻¹). Significant declining trends in icy days (–2.24 days decade⁻¹) and frosty nights (–3.35 days decade⁻¹) are found in the northwest of north China (105–115°E, 35–42°N). Frosty nights have also decreased significantly over northeastern China (–3.52 days decade⁻¹) and the Yangtze–Huaihe River basin (–4.22 days decade⁻¹). Figure 2 displays the time evolution of the observed and simulated frequency anomalies of the four indices in eastern China. The observed changes in extreme temperatures keep pace with the multi-model-simulated responses to ALL forcing, but not with the simulated responses to NAT forcing. We first apply the optimal fingerprinting



method (Allen and Tett 1999) to scale the modeled time series of extreme temperatures in eastern China with ALL forcing to best fit the observations. As shown in figure 3, one-signal analysis suggests that climate models with ALL forcing can reproduce the observed frequency changes in summer days and icy days well, and have scaling factor estimates consistent with the value one though bear certain internal variability. However, climate models tend to overestimate (underestimate) the frequency change in tropical

nights (frosty nights). This implies that models perform better in simulating the observed frequency change in daytime extreme temperatures than nighttime extremes. Though focusing on percentile-based extreme temperatures, Lu *et al* (2016) also found that climate models with ALL forcing do a better job in reproducing the frequency changes in daytime extreme indices than nighttime indices. It may be associated with the model's deficiency in reproducing the seasonality of warming trends in T_{\min} in eastern China.

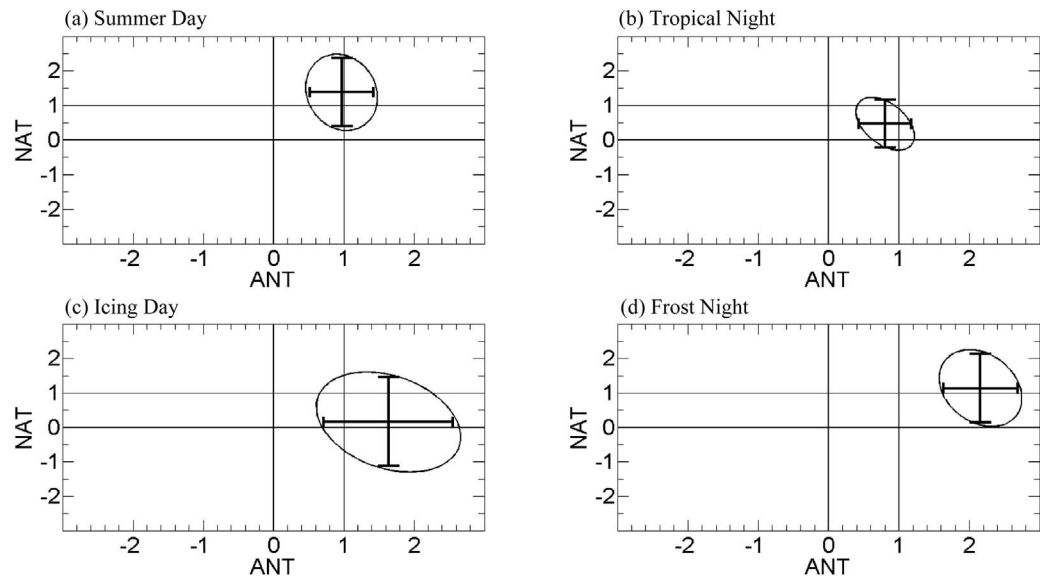


Figure 4. Scaling factors for changes in the annual frequencies of the four extreme temperature indices. Best estimates of the scaling factors that scale ANT and NAT signal patterns in two-signal detection analysis to best reproduce the observed annual anomalies of the frequency of extreme temperatures. The vertical bars mark the 5%–95% uncertainty range for each signal, and the ellipses mark the two-dimensional 90% confidence region.

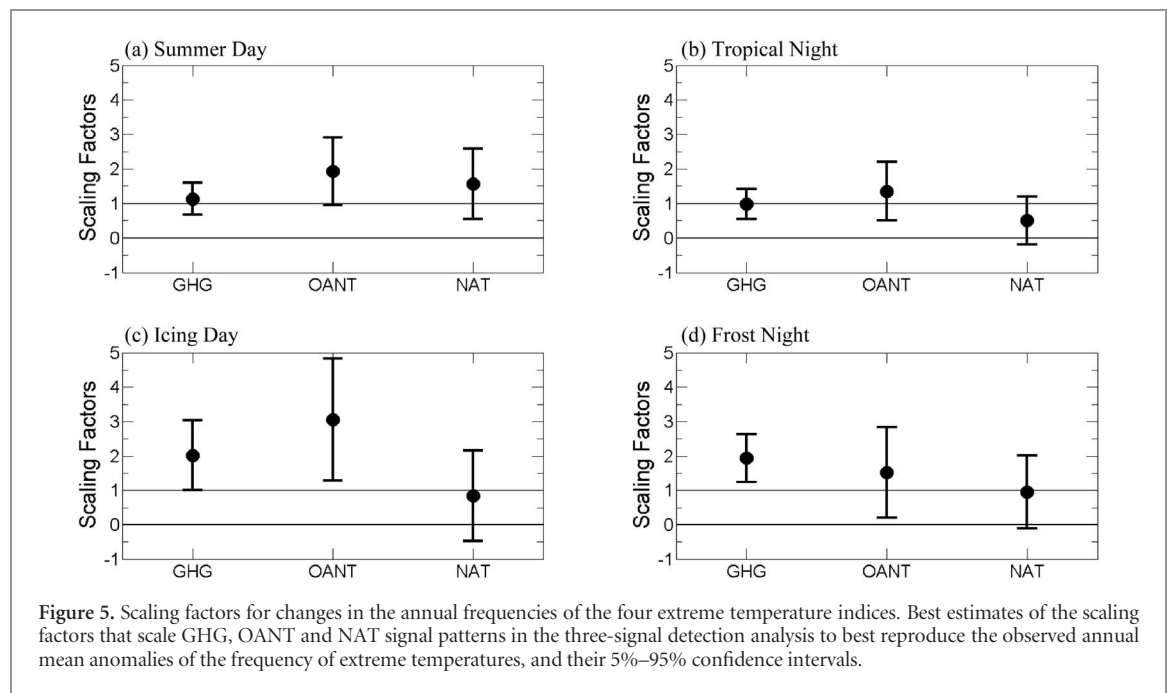
Lewis and Karoly (2013) found that the T_{\min} trends are noticeably subdued by the CMIP5 models, particularly in the boreal winter, when shallow boundary layers and soil freeze/thaw cycles are likely difficult to be simulated realistically. On the other hand, direct visual inspection of figure 3 illustrates that the uncertainty ranges in the scaling factors for cold extremes are larger than warm extremes, which implies smaller variability in the frequency of simulated cold extremes than that of observed ones. Other studies also found similar result existing in the changes in the annual maxima and minimum of daily temperatures (Morak *et al* 2013, Wen *et al* 2013, Yin *et al* 2017). A possible cause for this is that the strong internal variability of winter extreme temperatures in eastern China was underestimated by the CMIP5 climate models (figure 2 and figure S7). Increased GHGs enhance downward longwave radiation and hence increase the surface air temperature and change the frequency of temperature extremes. Meanwhile, the increased water vapor in warmer atmosphere can further increase downward longwave radiation. However, other anthropogenic forcing agents (e.g. aerosols) can decrease daytime temperature and change the frequency of daytime extremes directly by obstructing downward solar radiation and indirectly by changing the properties of clouds. Natural forcing agents, such as solar variability and volcanic eruptions, may also lead to the variations of surface air temperature and change the frequency of extreme temperatures by modulating solar radiation at the surface and the interaction between aerosols and clouds. The respective roles of anthropogenic and natural forcings in the change of extreme temperatures remain to be elucidated.

3.2. Two-signal detection analysis

To detect the effects of ANT and NAT forcings in the same framework, we conduct two-signal detection analysis. As shown in figure 4, the 5%–95% uncertainty ranges of ANT scaling factors for the four indices do not include zero and the 90% confidence ellipse regions do not cover the origin of x - y coordinates. This indicates that the effect of ANT forcings can be clearly detected, and the climate responses of ANT and NAT forcings can be well separated from each other. In other words, the influence of human activities is detectable in the frequency changes of these four temperature extreme indices. Except for summer days and frosty nights, the 5%–95% uncertainty ranges of NAT scaling factors for other two indices include zero, suggesting that the effects of NAT forcings on their frequency changes are undetectable.

3.3. Three-signal detection analysis

To examine the influences of individual groups of anthropogenic forcing agents, we conduct three-signal analysis to scale the model responses of GHG, OANT (ALL minus the sum of GHG and NAT) and NAT for the optimal agreement with observed frequency changes in extreme temperatures. As shown in figure 5, the results reveal that the effects of anthropogenic increase in GHGs can be clearly detected in the frequency changes of these four indices. Models appear to underestimate the effects of GHGs on the changes in icy days and frosty nights by a factor close to two. It is inferred that the model's deficiency in the effects of GHGs on the changes in cold-season extreme temperatures is associated with an underestimation of GHG-forced temperature changes in the cold season in eastern China. Morak *et al* (2013) found that



the HadGEM1 model significantly underestimates the changes in extreme temperatures in winter across large parts of Asia. Chen and Frauenfeld (2014) found that the winter warming in the CMIP5 models is only about half (one-fourth) of the observed warming in China for the period of 1901–1999 (1950–1999). The effects of OANT are also detectable, but with larger uncertainty. For all extremes indices, OANT effects are underestimated by the models. This may be due to the omission or simplification of the indirect effects of anthropogenic aerosols in some climate models, such as CanESM2 and IPSL-CM5A-LR (Hu *et al* 2014). Except for summer days, the influence of NAT forcings on other indices cannot be detected. These analyses demonstrate that the human-induced rise in greenhouse gas has imposed a detectable impact on the frequency change in extreme temperatures over eastern China.

3.4. Attribution

Based on the estimate results of three-signal analyses, we quantify contributions to the frequency changes of extreme temperatures to individual factors through multiplying the simulated trends in GHG, OANT and NAT signals by the respective scaling factors. As shown in figure 6, we find that the observed frequency changes in extreme temperatures are the net result of the counteracting effects from GHG and OANT forcing agents, since NAT forcing imposes little influence on these changes. Among three individual components of ALL forcings, the effect of anthropogenic emission of GHGs is dominant and has changed the frequencies of summer days (tropical nights, icy days, frosty nights) by rates of $+3.48 \pm 1.45$ ($+2.99 \pm 1.35$, -2.52 ± 1.28 , -4.11 ± 1.48) days decade⁻¹. Other anthropogenic forcing agents (dominated by anthropogenic aerosols) partly offset the effect from

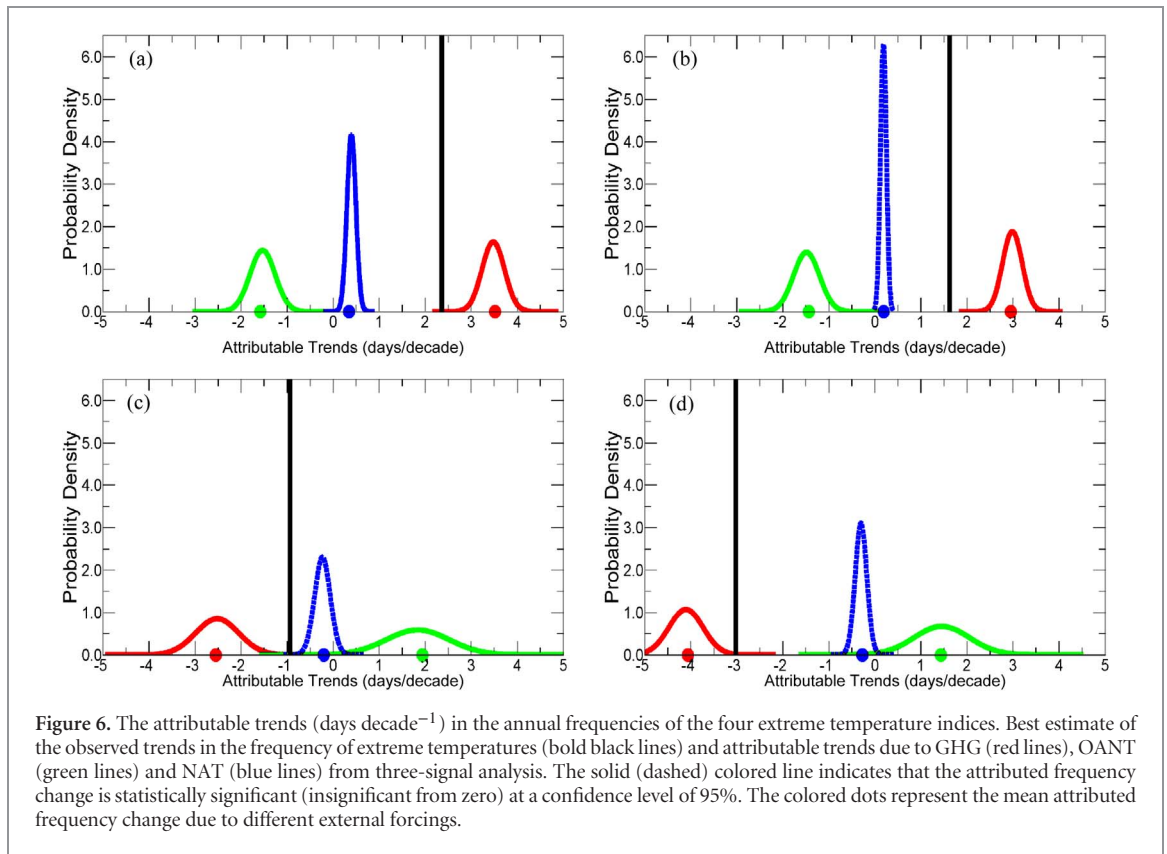
GHGs and changed the frequencies of these four indices by -1.53 ± 0.78 , -1.49 ± 0.94 , $+1.84 \pm 1.07$, $+1.45 \pm 1.26$ days decade⁻¹, respectively.

3.5. Robustness test

To further evaluate the robustness of above results, we repeat these analyses based on the 5-year-mean series. As shown in figure S9, results from two-signal detection analyses are generally in line with those with 3-year-mean series. The influence of human activities can be clearly detected in the observed frequency changes of the four extreme indices. However, the effects of NAT forcing can no longer be detected in the change in summer days and frosty nights. Three-signal detection analyses based on 5-year-mean series also indicate that ANT influences (GHG and OANT) are detectable in the frequency changes of extreme temperatures (figure S10). And the influence of natural forcings cannot be robustly detected in any indices. All the detection analyses suggest that anthropogenic influences are responsible for the observed frequency changes of these four temperature extreme indices.

4. Summary

In this study, we use an optimal fingerprinting method to compare the observed and multi-model-simulated frequency changes in four absolute extreme temperatures indices in eastern China for the period 1960–2012. Our detection analyses include two-signal analysis using climate responses to ANT and NAT forcings, and three-signal analysis using the signals of GHG, OANT and NAT forcings. We find that the influences of human activities and natural external forcing can be clearly separated from each other. The anthropogenic influences on the frequency changes of extreme



temperatures can be detected both in two-signal and three-signal detection analyses. The influence of natural forcings cannot be robustly detected in any indices. This indicates that only the effects of human activities can explain observed frequency changes in extreme temperatures in eastern China.

We further quantify the contributions of GHG, OANT and NAT forcings to the observed frequency trends of absolute extreme temperatures in eastern China during 1960–2012. Results show that the influence of GHGs are dominant in the observed changes in extreme temperatures, and part of which are offset by the effects of other anthropogenic forcing agents. The combined effects of GHG and OANT forcings explain most of observed changes in the frequencies of extreme temperatures, since the contributions of NAT forcing are quite small in the long-term changes of extreme temperatures in eastern China.

It is worth pointing out some caveats of uncertainty existing in this study, which deserve future consideration. One source of uncertainty is the systematic bias in the mean state of surface air temperature between observations and simulations. We use elevation data and spatiotemporal-varying temperature lapse rates to correct the topography-related bias in the climatological mean annual cycle of each grid box. However, model simulations still have a small systematic bias in the climatological annual mean temperature in eastern China (figures S5 and S6). This discrepancy may partly be attributed to regional land use change, which may have substantial effect on the observed change in extreme temperatures. The previous study suggested

that the effects of land use change were detectable from other anthropogenic forcings on a quasi-global scale (Christidis *et al* 2013). For eastern China, the most typical land use change is urbanization, which could change the climatology and long-term trend of near-surface air temperature. However, it remains controversial as to how urbanization has contributed to the observed warming trends in Chinese urban stations (Wang and Yan 2016, Sun *et al* 2016, Ren *et al* 2017). A recent study quantified the relationship between trends in urban fraction and local urban warming rates in temperature records in China (Wang *et al* 2017). They found that regional average trend of urban-related warming in eastern China is less than 10% of overall warming trend. Nevertheless, a robust technique used for correcting local urban warming bias in temperature records is urgently required for the detection and attribution of climate change in rapidly urbanizing regions.

Our conclusions based on trend attribution analyses are consistent with the case studies of event attribution of recent extreme hot and cold temperatures in eastern China: anthropogenic influence has caused a substantial increase (decrease) in the likelihood of extreme hot (cold) temperatures (Sun *et al* 2014, Qian *et al* 2017). In summer 2017, many densely populated and economically developed cities in eastern China suffered extremely hot temperatures for more than 2 weeks. The city of Shanghai even experienced a record-breaking high temperature on 21 July 2017 since the establishment of the benchmark meteorological station (Xujiahui) in 1872. The rapid development

of urbanization in the region might further enhance the heatwave events in urban areas (Wang *et al* 2017). Undoubtedly, human-induced increase in extreme hot temperatures, combined with the explosive growth in population and wealth, will cause enhanced risks for ecosystems, agriculture, energy production and human health if timely and sufficient adaptation measures are not taken.

Acknowledgments

This study was supported by the National Key R&D Program of China (2016YFA0602501). JW was supported by the China Postdoctoral Science Foundation (2015M580122). SFBT was supported by CSSP-China and NCAS-Climate (R8/H12/83/029). ZY acknowledges the support from the National Natural Science Foundation of China (41475078) and JF acknowledges the support from the National Key R&D Program of China (2016YFA0600403).

ORCID iDs

Jun Wang  <https://orcid.org/0000-0002-9429-6484>

References

- Alexander L V *et al* 2006 Global observed changes in daily climate extremes of temperature and precipitation *J. Geophys. Res.* **111** D05109
- Allen M R and Tett S F B 1999 Checking for model consistency in optimal fingerprinting *Clim. Dyn.* **15** 419–34
- Bai L *et al* 2014 The effects of summer temperature and heat waves on heat-related illness in a coastal city of China, 2011–2013 *Environ. Res.* **132** 212–9
- Basu R and Samet J M 2002 Relation between elevated ambient temperature and mortality: a review of the epidemiologic evidence *Epidemiol. Rev.* **24** 190–202
- Chen L and Fraunfeld O W 2014 Surface air temperature changes over the twentieth and twenty-first centuries in China simulated by 20 CMIP5 models *J. Clim.* **27** 3920–37
- Christidis N, Stott P A, Brown S, Hegerl G C and Caesar J 2005 Detection of changes in temperature extremes during the second half of the 20th century *Geophys. Res. Lett.* **32** L20716
- Christidis N, Stott P A and Brown S J 2011 The role of human activity in the recent warming of extremely warm daytime temperatures *J. Clim.* **24** 1922–30
- Christidis N, Stott P A, Hegerl G C and Betts R A 2013 The role of land use change in the recent warming of daily extreme temperatures *Geophys. Res. Lett.* **40** 589–94
- Christidis N, Stott P A and Zwiers F W 2015 Fast-track attribution assessments based on pre-computed estimates of changes in the odds of warm extremes *Clim. Dyn.* **45** 1547
- Hegerl G C, Zwiers F W, Stott P A and Kharin V V 2004 Detectability of anthropogenic changes in annual temperature and precipitation extremes *J. Clim.* **17** 3683–700
- Hu N, Li L and Wang B 2014 The role of the aerosol indirect effect in the Northern Indian ocean warming simulated by CMIP5 models *Atmos Oceanic Sci. Lett.* **7** 411–6
- Field C B *et al* 2012 *Managing the Risks of Extreme Events and Disasters to Advance Climate Change Adaptation* (Cambridge: Cambridge University Press)
- Kim Y H *et al* 2016 Attribution of extreme temperature changes during 1951–2010 *Clim. Dyn.* **46** 1769
- Lesk C, Rowhani P and Ramankutty N 2016 Influence of extreme weather disasters on global crop production *Nature* **529** 84–7
- Lewis S C and Karoly D J 2013 Evaluation of historical diurnal temperature range trends in CMIP5 models *J. Clim.* **26** 9077–89
- Li X *et al* 2013 Near-surface air temperature lapse rates in the mainland China during 1962–2011 *J. Geophys. Res. Atmos.* **118** 7505–15
- Li Z and Yan Z 2009 Homogenized daily mean/maximum/minimum temperature series for China from 1960–2008 *Atmos. Oceanic Sci. Lett.* **2** 237–43
- Li Z, Cao L, Zhu Y and Yan Z 2016 Comparison of two homogenized datasets of daily maximum/mean/minimum temperature in China during 1960–2013 *J. Meteorol. Res.* **30** 53–66
- Lu C, Sun Y, Wan H, Zhang X and Yin H 2016 Anthropogenic influence on the frequency of extreme temperatures in China *Geophys. Res. Lett.* **43** 6511–8
- Morak S, Hegerl G C and Kenyon J 2011 Detectable regional changes in the number of warm nights *Geophys. Res. Lett.* **38** L17703
- Morak S, Hegerl G C and Christidis N 2013 Detectable changes in the frequency of temperature extremes *J. Clim.* **26** 1561–74
- Qian C, Wang J, Dong S, Yin H, Burke C, Ciavarella A, Dong B, Freychet N, Lott F C and Tett S 2017 Human influence on the record-breaking cold event in january of 2016 in Eastern China *Bull. Am. Meteorol. Soc.* (<https://doi.org/10.1175/BAMS-D-16-0138.1>)
- Ren G, Ding Y and Tang G 2017 An overview of mainland China temperature change research *J. Meteorol. Res.* **31** 3–16
- Ribes A, Azais J-M and Planton S 2009 Adaptation of the optimal fingerprint method for climate change detection using a well-conditioned covariance matrix estimate *Clim. Dyn.* **33** 707–22
- Ribes A, Planton S and Terray L 2013 Application of regularised optimal fingerprinting to attribution. Part I: method, properties and idealised analysis *Clim. Dyn.* **41** 2817–36
- Stott P A, Stone D A and Allen M R 2004 Human contribution to the European heatwave of 2003 *Nature* **432** 610–3
- Stott P A *et al* 2016 Attribution of extreme weather and climate-related events *WIREs Clim. Change* **7** 23–41
- Sun Q, Miao C and Duan Q 2015 Comparative analysis of CMIP3 and CMIP5 global climate models for simulating the daily mean, maximum, and minimum temperatures and daily precipitation over China *J. Geophys. Res. Atmos.* **120** 4806–24
- Sun Y *et al* 2014 Rapid increase in the risk of extreme summer heat in eastern China *Nat. Clim. Change* **4** 1082–5
- Sun Y *et al* 2016 Contribution of urbanization to warming in China *Nat. Clim. Change* **6** 706–9
- Trenary L, Delsole T, Tippet M K and Doty B 2015 Was the cold eastern US winter of 2014 due to increased variability? In explaining extremes of 2014 from a climate perspective *Bull. Am. Meteorol. Soc.* **96** S15–9
- Wang J and Yan Z 2016 Urbanization-related warming in local temperature records: a review *Atmos. Oceanic Sci. Lett.* **9** 129–38
- Wang J, Yan Z, Quan X and Feng J 2017 Urban warming in the 2013 summer heat wave in eastern China *Clim. Dyn.* **48** 3015–33
- Wang J, Tett S F B and Yan Z 2017 Correcting urban bias in large-scale temperature records in China, 1980–2009 *Geophys. Res. Lett.* **44** 401–8
- Wang S *et al* 2017 Accelerated increase in the Arctic tropospheric warming events surpassing stratospheric warming events during winter *Geophys. Res. Lett.* **44** 3806–15
- Wen H, Zhang X, Xu Y and Wang B 2013 Detecting human influence on extreme temperatures in China *Geophys. Res. Lett.* **40** 1171–6
- Yin H, Sun Y, Wan H, Zhang X and Lu C 2017 Detection of anthropogenic influence on the intensity of extreme temperatures in China *Int. J. Climatol.* **37** 1229–37
- Zhang X *et al* 2011 Indices for monitoring changes in extremes based on daily temperature and precipitation data *WIREs Clim. Change* **2** 851–70
- Zhou C and Wang K 2016 Coldest temperature extreme monotonically increased and hottest extreme oscillated over Northern Hemisphere land during last 114 years *Sci. Rep.* **6** 25721